LETTERS
PUBLISHED ONLINE: 1 NOVEMBER 2009 | DOI: 10.1038/NNANO.2009.302
nature nanotechnology

True solutions of single-walled carbon nanotubes for assembly into macroscopic materials

Virginia A. Davis[1,2†], A. Nicholas G. Parra-Vasquez[1,2‡], Micah J. Green[1,2†‡], Pradeep K. Rai[1,2‡], Natnael Behabtu[1,2], Valentin Prieto[1,2], Richard D. Booker[1], Judith Schmidt[4], Ellina Kesselman[4], Wei Zhou[5], Hua Fan[1], W. Wade Adams[1], Robert H. Hauge[1,3], John E. Fischer[5], Yachin Cohen[4], Yeshayahu Talmon[4], Richard E. Smalley[1,3§] and Matteo Pasquali[1,2,3*]

Translating the unique characteristics of individual single-walled carbon nanotubes into macroscopic materials such as fibres and sheets has been hindered by ineffective assembly. Fluid-phase assembly is particularly attractive, but the ability to dissolve nanotubes in solvents has eluded researchers for over a decade. Here, we show that single-walled nanotubes form true thermodynamic solutions in superacids, and report the full phase diagram, allowing the rational design of fluid-phase assembly processes. Single-walled nanotubes dissolve spontaneously in chlorosulphonic acid at weight concentrations of up to 0.5wt%, 1,000 times higher than previously reported in other acids. At higher concentrations, they form liquid-crystal phases that can be readily processed into fibres and sheets of controlled morphology. These results lay the foundation for bottom-up assembly of nanotubes and nanorods into functional materials.

The lack of scalable assembly methods has been a key block in the manufacture of functional nanomaterials. Fluid-phase assembly is the most promising method for producing large, ordered structures of nano-objects[1,2]. Single-walled carbon nanotubes (SWNTs) are a particularly important and challenging case, and are a model system for nanorods. Based on single-object data, the thermal, electrical and mechanical properties of SWNTs are unique[3] and could be of use in numerous breakthrough applications such as multifunctional high-strength fibres, coatings and transparent conducting films. However, macroscopic SWNT materials demonstrate only a small fraction of the possible single-object properties, largely because of their ineffective assembly, for example, into fibres and sheets[4–11]. Successful assembly begins with control of dispersion and phase behaviour and requires a scientific understanding of flow, colloidal interactions and solvent removal. (Note that an SWNT 'dispersion' comprises a homogeneous suspension or dissolution of SWNTs and/or small SWNT aggregates, and SWNT 'phase behaviour' refers to the various liquid microstructures that can form as a function of SWNT and solvent parameters.) The dispersion and phase behaviour properties of SWNTs in liquids are particularly complex compared with those of other anisotropic nanomaterials and rod-like polymers. Inorganic nanorods such as TiO_2 and CdSe (ref. 12) can be synthesized to have uniform size and electronic properties and are readily dispersed in organic solvents. In contrast, SWNTs have a broad distribution of length and electronic properties, and their high aspect ratio (greater than ~500) and strong van der Waals attraction[13] make dispersion exceedingly difficult. Most SWNT fluids are surfactant-stabilized suspensions achieved through sonication[10], although SWNTs can also be dispersed via sidewall functionalization[14] or reduction using alkali metals[15]. The dissolution of a few parts per million of pristine SWNTs in *N*-methylpyrrolodine (NMP) is a recent major achievement[16]. Liquid-crystalline solutions of carbon nanotubes (CNTs) have been achieved in a few cases by inducing repulsion between the CNTs. Sidewall-functionalized multiwalled nanotubes (MWNTs) form liquid crystals in water[17,18], and pristine SWNTs form liquid crystals in superacids[19] and in water when stabilized by acids containing hydrophobic groups[20], or when trapped in temperature-sensitive crosslinked hydrogels[21]. Stabilization and functionalization techniques are not optimal for materials processing because functionalization disrupts the electronic properties of SWNTs and stabilization introduces non-SWNT material into the final product. Phase transitions have been determined semi-quantitatively by cross-polarized optical microscopy, but the effect of solvent quality on phase transitions has not been studied. Based on initial observations[19,22,23], the phase diagram describing the liquid-crystalline behaviour of carbon nanotubes is very complex and requires the control and understanding of nanotube–solvent interactions.

Here, we present a complete experimental phase diagram of SWNTs in superacids. We also compare it with our recent theory of polydisperse rods and competing short-range repulsion and long-range attraction[24].

The centre panel of Figure 1 shows the first phase diagram of a dispersion of nanorods, presenting the effects of both solvent quality and concentration. The phase diagram portrays purified SWNTs in mixtures of sulphuric and chlorosulphonic acid of varying acidity, that is, solvent quality, measured by SWNT protonation (Supplementary Fig. S1).

Traversing the phase diagram from left to right (low concentration to high concentration of rods, constant solvent quality) results in a transition from an isotropic (I) phase (randomly oriented rods) to a biphasic system in which the isotropic phase is in equilibrium with a liquid-crystalline (LC) phase, and then to a single liquid-crystalline phase composed of domains randomly oriented with respect to each other. The concentration ϕ_i of the

[1]Richard E. Smalley Institute for Nanoscale Science and Technology, Rice University, Houston, Texas 77005, USA, [2]Department of Chemical and Biomolecular Engineering, Rice University, Houston, Texas 77005, USA, [3]Department of Chemistry, Rice University, Houston, Texas 77005, USA, [4]Department of Chemical Engineering, Technion–Israel Institute of Technology, Haifa 32000, Israel, [5]Department of Material Science and Engineering, University of Pennsylvania, Philadelphia, Pennsylvania, USA; †Present address: Department of Chemical Engineering, Auburn University, Auburn, Alabama 36849, USA (V.A.D.); Department of Chemical Engineering, Texas Tech University, Lubbock, Texas 79409, USA (M.J.G.); ‡These authors contributed equally to this work; §Deceased 28 October 2005. *e-mail: mp@rice.edu

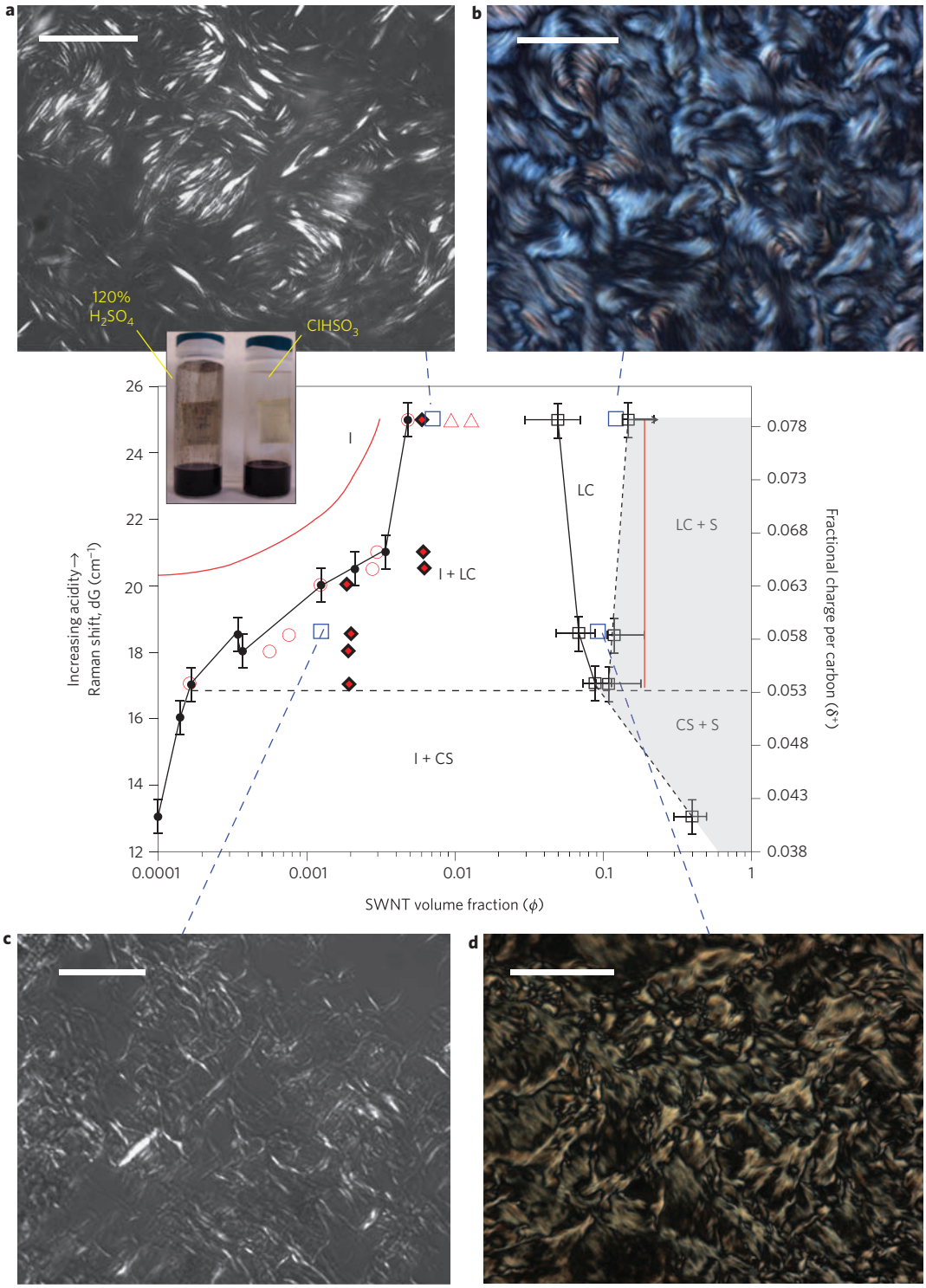

Figure 1 | Phase diagram of SWNTs in superacids and cross-polarized light micrographs showing the effect of solvent quality and SWNT concentration on microstructure. Phases include isotropic (I), liquid-crystalline (LC), crystal solvate (CS) and solid (S). Solvent quality is quantified by fractional charge per carbon, measured by the shift dG of the Raman G peak of SWNTs (514 nm laser). Black symbols denote experimental results and red symbols refer to model predictions[24]. Circles designate the isotropic concentration ϕ_i from experiment (filled circles) and model (open circles). Black and red diamonds indicate the initial system concentration before phase separation. Open red triangles indicate ϕ_i and ϕ_n in a system of monodisperse hard-rods (Onsager). Red lines are the model predictions of the isotropic and liquid-crystalline stability limits, that is, cloud curves. Black dotted lines connect the experimental data points to denote experimental phase boundaries such as the LC/LC + S vertical boundary, the LC + S/CS + S horizontal boundary, and the I + LC/I + CS diagonal boundary. An LC + CS regime may also exist within the shaded region, as suggested by Papkov[33]. **a–d**, Light microscopy shows morphology just inside the biphasic region at 1.21 vol% in $ClSO_3H$ (**a**), 0.132 vol% in 120% H_2SO_4 (**c**), and in the liquid-crystalline phase at 12.1 vol% in $ClSO_3H$ (**b**) and 10.6 vol% in 120% H_2SO_4 (**d**). Liquid-crystalline domains are larger, defect density is lower, and domain orientation changes more gradually in $ClSO_3H$ (**b**) than in 120% H_2SO_4 (**d**). Scale bars: 50 μm (**a**) and 20 μm (**b–d**). Errors in measurements of ϕ_i are ±5%. Errors in measurement for ϕ_n are ±2%.

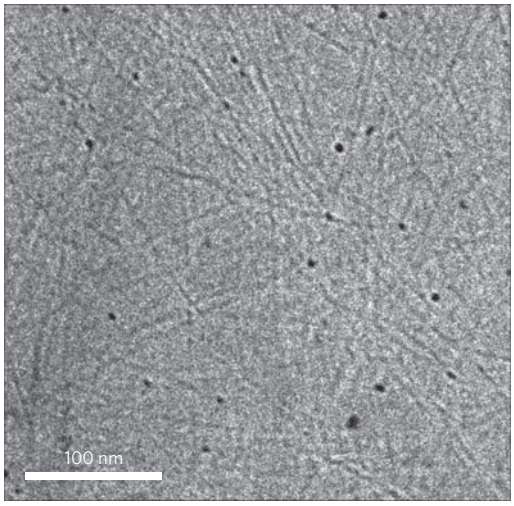

Figure 2 | Cryo-TEM image of SWNTs (0.134 vol%) in chlorosulphonic acid. The SWNTs are individually dispersed and form an isotropic phase. Dark, black dots are left-over catalyst particles.

isotropic phase in equilibrium with the aligned phase grows with increasing fractional charge (better solvent quality), in accordance with classical theories[25]. In chlorosulphonic acid (the highest fractional charge on SWNTs), ϕ_i was measured to be ~0.61 vol%, which is the highest reported solubility of pristine SWNTs to date, equivalent to ~1,000× their solubility in NMP (Supplementary Movie S1). Cryo-transmission electron microscopy (cryo-TEM) of 0.134 vol% SWNTs in chlorosulphonic acid (Fig. 2) reveals individual SWNTs (Supplementary Fig. S3) forming an isotropic concentrated phase. This is the first image of pristine SWNTs individually dissolved in a single-component fluid, as well as the first cryo-TEM imaging of a superacid solution. In contrast to classical systems such as rod-like polymers or tobacco mosaic virus in water, SWNTs display a new feature in the phase diagram: in poor solvents, the dilute isotropic phase, that is, non-interacting SWNTs in solution, coexists with a concentrated liquid-crystalline phase rather than with a solid phase as described by Flory's lattice theory[25] and Khokhlov's extension of Onsager theory[26]. Moreover, the liquid-crystalline domains show a peculiar 'endless strand' (spaghetti-like) morphology in the biphasic region. Below a critical solvent quality (Raman shift, dG, of less than ~17 cm^{-1}, corresponding to ~100% H_2SO_4), the liquid-crystalline phase is lost as a result of attractive interactions, yielding an isotropic phase with a minuscule rod concentration in equilibrium with a high-concentration solid phase (probably a crystal solvate, labelled 'CS' in the phase diagram).

The LC phase consists of seemingly endless birefringent strands that can flow and coalesce into larger domains. In contrast, the solid phase consists of aligned SWNTs intercalated by a minimal amount of acid. As in many colloidal systems, the morphology of the CS phase depends on the order and rate of the addition of the components. Adding water slowly to a dispersion of SWNTs in fuming sulphuric acid lowers the acidity and destabilizes the SWNTs, which aggregate into discrete tactoids (elongated particles termed 'alewives'); these structures do not form when SWNTs are mixed directly with aqueous acid[22].

At sufficiently high acidity (dG > 17 cm^{-1}) and SWNT concentration, the system becomes completely liquid crystalline. The critical concentration ϕ_n (indicated by black squares in the phase diagram) was determined using information from light microscopy, dynamic rheometry, steady shear rheometry and differential scanning calorimetry (Supplementary Figs S4–S7, Movie S2). As long as the solvent is sufficiently acidic, ϕ_n depends weakly on acid strength, in contrast to ϕ_i. However, acidity controls the morphology of the liquid crystal: higher acidity yields larger domains with fewer defects (compare Fig. 1b and d), and therefore will yield macroscopic materials with higher microstructural order and better properties. The coexistence of a dilute isotropic phase with a liquid-crystalline phase at low acidity (17 cm^{-1} < dG < 20 cm^{-1}, $\phi_n \approx 10\%$) is remarkably different from the behaviour of rod-like polymers (described by Flory-like lattice theories[25]), in which the dilute isotropic phase is in equilibrium with a solid crystal solvate. Neither Onsager's excluded-volume theory[27] (open triangles in Fig. 1) nor subsequent refinements that account for solvent quality[26] and polydispersity[28,29] can capture the observed trends for ϕ_i and ϕ_n. The SWNT/superacid system consists of concentrated phases of rod-like molecules with competing short-range repulsion (for example, electrostatic) and long-range attraction (for example, van der Waals or depletion) between parallel rods; these forces are often present in colloidal systems such as dilute electrolytes, which can be described in terms of Derjaguin–Landau–Verwey–Overbeek (DLVO) theory[30,31]. However, none of these theories describes concentrated phases of rod-like molecules with both long-range attractive and repulsive interactions[32].

Our recent study extends the Onsager model to include polydispersity (as in refs 28,29), long-range attraction (to model van der Waals forces) and short-range repulsion (to capture electrostatic forces)[24]. Interactions are modelled through a phenomenological square-well potential. As acid strength decreases, protonation drops such that van der Waals forces outweigh electrostatic forces, yielding an effective long-range attraction. These results show that the isotropic–biphasic stability limit (left red line in Fig. 1) drops by several orders of magnitude as the acid strength decreases. To the right of this line, the two phases coexist. The nematic–biphasic limit (right red line) is unaffected by acid strength, in contrast with the Flory prediction. Simply stated, long-range attraction pulls the rods out of the isotropic phase, but electrostatic repulsion prevents their collapse into a solid. A point-by-point comparison between theory (red circles) and experiment (black circles) reveals a close match for the isotropic concentration after phase separation (with the starting concentration indicated by red and black diamonds). This match between theory and experiment confirms that the behaviour of SWNT/superacid systems is caused by the solvent-mediated competition of short-range repulsion and long-range attraction. It is also notable that the isotropic concentration in chlorosulphonic acid matches the theoretical prediction for athermal solvents from Wensink and Vroege[29], indicating that van der Waals interactions are fully counterbalanced and that chlorosulphonic acid is indeed the elusive athermal solvent for SWNTs.

At still higher concentrations the system undergoes a transition to a mixture of liquid-crystalline and solid (S, consisting of undispersed SWNT ropes) phases. This occurs at $\phi = 11$ vol% in sulphuric acid, but has not been observed in chlorosulphonic acid at concentrations up to 17 vol%. Comparable values for the transition to the LC + S region are suggested by experiments where solution-spun SWNT fibres were placed in various super acids and swollen by superacid intercalation[7]. Remarkably, immersing solid samples of SWNTs (for example, spun fibres, cast films) in chlorosulphonic acid resulted in complete, spontaneous dissolution of the SWNTs (Supplementary Fig. S9, Movies S3–S5). The overall I/LC/CS/S topology of the SWNT/acid phase diagram is similar to that described by Papkov for rigid-chain polymers[33]. Papkov's analysis also suggests the existence of an LC + CS regime. Such a regime is difficult to detect experimentally, and may well exist within the shaded solid (S) region of the SWNT/acid phase diagram.

Controlling the liquid-crystalline phase behaviour of SWNTs in superacids has significant practical importance. Fibres and films can be formed readily by flow-processing liquid-crystalline SWNT acid dopes (high SWNT concentration mixtures) and quenching the acid

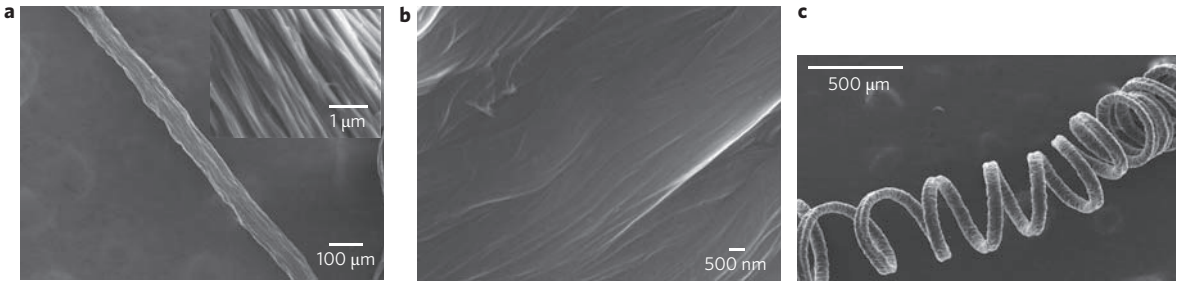

Figure 3 | Dispersions of SWNTs (10.8 vol%) in sulphuric acid processed using different coagulation conditions. a, Straight fibre coagulated in water, showing hierarchical microstructure of bundles (detail shown in inset). **b**, Film slowly evaporated in anhydrous air, showing a smooth microstructure. **c**, Coiled and pleated fibre coagulated in ether.

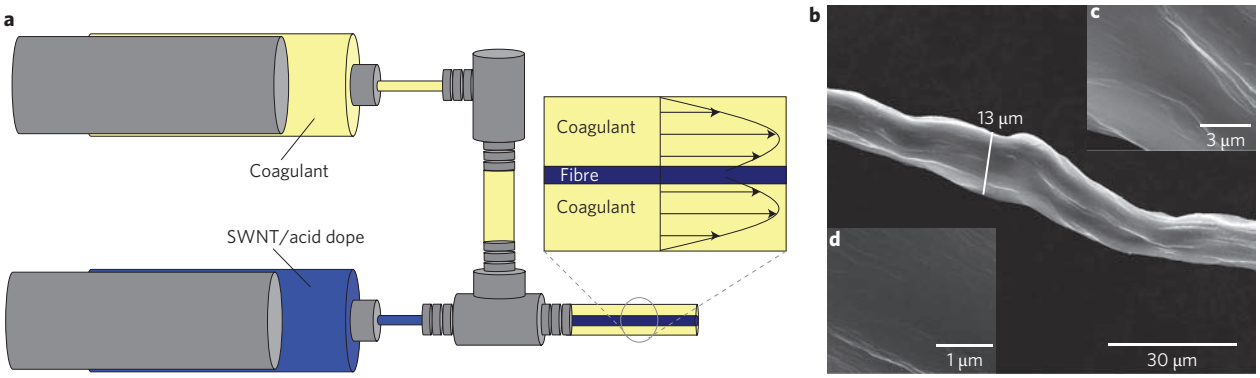

Figure 4 | Fibre spun from 8.5 vol% SWNTs in pure chlorosulphonic acid and coagulated in 96% aqueous sulphuric acid. a–d, The SWNT/acid dope is extruded into a coagulant flowing faster than the dope (**a**); this provides tension and draws the coagulating fibre, yielding thin fibres with a smooth surface (**b**). The uniform microstructure of the aligned fibrils (**c**,**d**) is the result of the large liquid-crystalline domains in the fluid dope.

in a process that is very similar to those used in the commercial spinning of high-performance aramidic fibres out of strong acids (DuPont's Kevlar^{TM} and Teijin's Twaron^{TM}; refs 7,9). The resulting materials inherit order and alignment from the parent liquid-crystalline phase. The viscosity of the dopes is at a minimum at $\phi \approx \phi_n$ (due to pre-existing alignment in the fluid phase), which facilitates flow processing. Moreover, solvent removal and the associated potential formation of voids and defects are minimized by working at high SWNT concentrations. Processing biphasic dispersions (I + LC) yields poorly ordered materials.

The phase diagram guides identification of the optimal starting fluid composition, and also provides insight into the solvent removal process (coagulation). Coagulation plays a key role in determining micro- and macrostructure of fibres and films. For example, fibres that are solution-spun from SWNTs in 102–123% H_2SO_4 and coagulated with water (a rapid coagulation path from a marginally good solvent to a poor solvent) display a hierarchical microstructure, in which small bundles (tens to hundreds of nanometres thick) of nanotubes combine into larger bundles (about a micrometre thick) to form the macroscopic fibre (Fig. 3a). This wet-spinning technique can easily produce tens of metres of continuous fibre in a matter of minutes, including the coiled structure in Fig. 3c. When the same dope is instead sandwiched between glass slides and the acid is evaporated (a slow coagulation process that occurs at constant solvent quality), the resultant film has a smooth, dense microstructure of coalesced bundles (Fig. 3b). The slinky-like fibre with a pleated structure (Fig. 3c) was produced by coagulating rapidly into ether (which forms a solid skin and allows coagulant to enter the proto-fibre), followed by drying the residual liquid slowly (which causes capillary compression). Pleated fibres are of interest for applications requiring high surface areas such as hydrogen storage[34] and absorption-based sensors[35]. Straight fibres are of interest for structural reinforcement, and smooth, dense films for electrical applications such as electrically conductive thin films.

Solution-spun fibres from 8.5 vol% SWNTs in pure chlorosulphonic acid display similar behaviour. Spinning the dope into a stagnant viscous coagulation bath of 96% sulphuric acid yields fibres uniformly composed of fine fibrils, with fewer small-scale defects than fibres spun from sulphuric acid; this is due to the more regular microstructure of the liquid-crystalline phase. Viscous forces at the coagulant–proto-fibre interface can cause surface buckling-like irregularities (Supplementary Fig. S10), which can be prevented by using a low-viscosity coagulant such as chloroform or dichloromethane or by co-flowing (as in ref. 5) the coagulant with the coagulating proto-fibre (Fig. 4) to yield fibres that combine a uniform microstructure with a regular, aligned macrostructure. Acid-spun fibres are well aligned, the typical ratio of parallel to perpendicular Raman intensity being ~15, with some fibres reaching a value of 28. Typical strength ranges from 50 to 150 MPa, with some spinning tests yielding a strength in excess of 320 MPa. The typical modulus is 120 GPa, and electrical resistivity is as low as 120 μΩ cm. All properties are probably limited because of the relatively short length (~500 μm) of the constituent SWNTs. These results highlight the combined importance of phase behaviour, flow and solvent removal in the assembly of macroscopic SWNT materials.

In conclusion, we now understand quantitatively the phase diagram of SWNTs in strong acids. The behaviour in chlorosulphonic acid dispels the deep-seated notion that SWNTs are essentially insoluble in any solvent: cryo-TEM shows the spontaneous formation of isotropic concentrated phases of individual SWNTs, and the isotropic–nematic phase boundaries are match predictions for length-polydisperse athermal rods[29]. Comparison against our recent extension of this model includes the competition of van der

Waals attraction and electrostatic repulsion in weaker acids and is able to capture the whole phase diagram. We have established that the microstructure of the liquid-crystalline phase as well as ensuing macroscopic fibres and films is directly linked to solvent quality. Stronger acids yield larger liquid-crystalline domains and more uniform fibres and films. Flow processing and coagulation also affect the final material morphology. These combined results place SWNT processing onto a solid scientific ground and are likely to encourage further the engineering of macroscopic nanotube materials. They will also have an impact on the numerous ongoing efforts for the combined bottom-up/top-down assembly of other cylindrical nanomaterials.

Received 13 July 2009; accepted 14 September 2009; published online 1 November 2009

References

1. Lieber, C. M. & Wang, Z. L. Functional nanowires. *MRS Bull.* **32,** 99–108 (2007).
2. Yu, G., Cao, A. & Lieber, C. M. Large-area blown bubble films of aligned nanowires and carbon nanotubes. *Nature Nanotech.* **2,** 372–377 (2007).
3. Baughman, R. H. Materials science—putting a new spin on carbon nanotubes. *Science* **290,** 1310–1311 (2000).
4. Chae, H. G. & Kumar, S. Materials science—making strong fibers. *Science* **319,** 908–909 (2008).
5. Dalton, A. B. *et al.* Super-tough carbon-nanotube fibres. *Nature* **423,** 703 (2003).
6. Duggal, R., Hussain, F. & Pasquali, M. Self-assembly of single-walled carbon nanotubes into a sheet by drop drying. *Adv. Mater.* **18,** 29–34 (2006).
7. Ericson, L. *et al.* Macroscopic, neat, single-walled carbon nanotube fibers. *Science* **305,** 1447–1450 (2004).
8. Li, Q. W., Zhu, Y. T. T., Kinloch, I. A. & Windle, A. H. Self-organization of carbon nanotubes in evaporating droplets. *J. Phys. Chem. B* **110,** 13926–13930 (2006).
9. Sreekumar, T. V. *et al.* Single-wall carbon nanotube films. *Chem. Mater.* **15,** 175–178 (2003).
10. Vigolo, B. *et al.* Macroscopic fibers and ribbons of oriented carbon nanotubes. *Science* **290,** 1331–1334 (2000).
11. Zhang, S. J., Koziol, K. K. K., Kinloch, I. A. & Windle, A. H. Macroscopic fibers of well-aligned carbon nanotubes by wet spinning. *Small* **4,** 1217–1222 (2008).
12. Li, L. S., Marjanska, M., Park, G. H. J., Pines, A. & Alivisatos, A. P. Isotropic-liquid crystalline phase diagram of a CdSe nanorod solution. *J. Chem. Phys.* **120,** 1149–1152 (2004).
13. Thess, A. *et al.* Crystalline ropes of metallic carbon nanotubes. *Science* **273,** 483–487 (1996).
14. Hudson, J. L., Casavant, M. J. & Tour, J. M. Water-soluble, exfoliated, nonroping single-wall carbon nanotubes. *J. Am. Chem. Soc.* **126,** 11158–11159 (2004).
15. Penicaud, A., Poulin, P., Derre, A., Anglaret, E. & Petit, P. Spontaneous dissolution of a single-wall carbon nanotube salt. *J. Am. Chem. Soc.* **127,** 8–9 (2005).
16. Bergin, S. D. *et al.* Towards solutions of single-walled carbon nanotubes in common solvents. *Adv. Mater.* **20,** 1876–1881 (2008).
17. Song, W. H. & Windle, A. H. Isotropic-nematic phase transition of dispersions of multiwall carbon nanotubes. *Macromolecules* **38,** 6181–6188 (2005).
18. Zhang, S. J., Kinloch, I. A. & Windle, A. H. Mesogenicity drives fractionation in lyotropic aqueous suspensions of multiwall carbon nanotubes. *Nano Lett.* **6,** 568–572 (2006).
19. Davis, V. A. *et al.* Phase behavior and rheology of SWNTs in superacids. *Macromolecules* **37,** 154–160 (2004).
20. Badaire, S. *et al.* Liquid crystals of DNA-stabilized carbon nanotubes. *Adv. Mater.* **17,** 1673–1676 (2005).
21. Islam, M. F. *et al.* Nematic nanotube gels. *Phys. Rev. Lett.* **92,** 088303 (2004).
22. Ramesh, S. *et al.* Dissolution of pristine single-walled carbon nanotubes in superacids by direct protonation. *J. Phys. Chem. B* **108,** 8794–8798 (2004).
23. Rai, P. K. *et al.* Isotropic-nematic phase transition of single-walled carbon nanotubes in strong acids. *J. Am. Chem. Soc.* **128,** 591–595 (2006).
24. Green, M. J., Parra-Vasquez, A. N. G., Behabtu, N. & Pasquali, M. Modeling the phase behavior of polydisperse rigid rods with attractive interactions with applications to single-walled carbon nanotubes in superacids. *J. Chem. Phys.* **131,** 084901 (2009).
25. Flory, P. J. Phase equilibria in solutions of rod-like particles. *Proc. R. Soc. London A* **234,** 73–89 (1956).
26. Khokhlov, A. R. in *Liquid Crystallinity in Polymers* (ed. Ciferri, A.) 97–129 (VCH Publishers, 1991).
27. Onsager, L. The effects of shape on the interaction of colloidal particles. *Ann. NY Acad. Sci.* **51,** 627–659 (1949).
28. Speranza, A. & Sollich, P. Isotropic-nematic phase equilibria in the Onsager theory of hard rods with length polydispersity. *Phys. Rev. E* **67,** 061702 (2003).
29. Wensink, H. H. & Vroege, G. J. Isotropic-nematic phase behavior of length-polydisperse hard rods. *J. Chem. Phys.* **119,** 6868–6882 (2003).
30. Israelachvili, J. N. *Intermolecular and Surface Forces* 2nd edn (Academic Press, 1992).
31. Chapot, D., Bocquet, L. & Trizac, E. Interaction between charged anisotropic macromolecules: application to rod-like polyelectrolytes. *J. Chem. Phys.* **120,** 3969–3982 (2004).
32. Dogic, Z., Purdy, K. R., Grelet, E., Adams, M. & Fraden, S. Isotropic-nematic phase transition in suspensions of filamentous virus and the neutral polymer dextran. *Phys. Rev. E* **69,** 051702 (2004).
33. Papkov, S. Liquid crystalline order in solutions of rigid-chain polymers. *Adv. Polym. Sci.* **59,** 75–102 (1984).
34. Leonard, A. D. *et al.* Nanoengineered carbon scaffolds for hydrogen storage. *J. Am. Chem. Soc.* **131,** 723–728 (2009).
35. Neimark, A. V., Ruetsch, S., Kornev, K. G. & Ravikovitch, P. I. Hierarchical pore structure and wetting properties of single-wall carbon nanotube fibers. *Nano Lett.* **3,** 419–423 (2003).

Acknowledgements

The authors acknowledge the help of R. Duggal, S. Ramesh, L. Ericson, C. Lupu, E. Whitsitt, R. Pinnick, C. Kittrell, W.-F. Hwang, H. Schmidt, B. Yakobson, J. Tour, K. Winey, K. Strong and B. Maruyama. Funding was provided by the Office of Naval Research under grant no. N00014-01-1-0789, AFOSR grant no. FA9550-06-1-0207, AFRL agreements FA8650-07-2-5061 and 07-S568-0042-01-C1, NSF CAREER, USA-Israel Binational Science Foundation, and the Evans-Attwell Welch Postdoctoral Fellowship. Cryo-TEM imaging was performed at the Hannah and George Krumholz Laboratory for Advanced Microscopy, part of the Technion Project on Complex Liquids, Nanostructure and Macromolecules.

Author contributions

V.A.D., M.J.G., M.P., A.N.G.P.V. and N.B. analysed the data and co-wrote the paper. M.J.G. and M.P. performed theoretical analysis and modelling. V.A.D., A.N.G.P.V., M.J.G., P.K.R., N.B., V.P. and W.Z. performed phase boundary experiments and A.N.G.P.V., N.B., M.J.G., R.D.B. and H.F. performed fibre and film experiments, all with direction and analysis from W.W.A., R.H., J.F., R.E.S. and M.P. J.S., E.K. and A.N.G.P.V. performed cryo-TEM experiments with direction and analysis from Y.C., Y.T. and M.P. All authors discussed the results and commented on the manuscript.

Additional information

Supplementary information accompanies this paper at www.nature.com/naturenanotechnology. Reprints and permission information is available online at http://npg.nature.com/reprintsandpermissions/. Correspondence and requests for materials should be addressed to M.P.